PAPER Nr.: 19

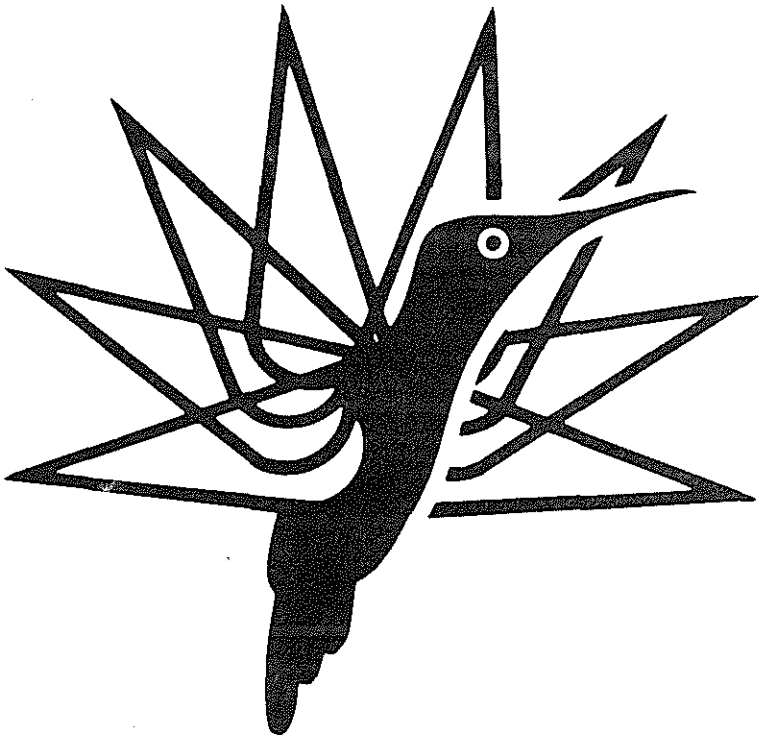

ROTOR LOADINGS IN HOVER - CORRELATION OF THEORY AND EXPERIMENT

P.C. TARTTELIN

FLIGHT DYNAMICS DIVISION
ROYAL AEROSPACE ESTABLISHMENT
BEDFORD MK41 6AE, UK

FIFTEENTH EUROPEAN ROTORCRAFT FORUM

SEPTEMBER 12 - 15, 1989 AMSTERDAM

ROTOR LOADINGS IN HOVER - CORRELATION OF THEORY AND EXPERIMENT

P.C. Tarttelin

Flight Dynamics Division
Royal Aerospace Establishment
BEDFORD MK41 6AE, UK

SUMMARY

This paper describes the analysis and results of a flight experiment designed to obtain estimates of rotor blade incidence and deformations from detailed flight test measurements at RAE Bedford using a Puma helicopter as the test vehicle. The focus of attention is on a series of hover flights; the derived results are evaluated to examine the contributions of blade vortex interaction, tail rotor interference, and blade deformation to the load distribution on the main rotor for a range of thrust coefficients. The accuracy of various derived parameters is discussed. The results are used to derive the inflow distribution at the rotor disc for one of these cases. The paper demonstrates the importance of blade vortex interaction and blade flexibility, and highlights the differences between the distribution of derived loading, and those obtained from a rotor loads prediction program. The general aim of the work is to support improvements to the representation of the rotor dynamics in the RAE generic simulation model.

1 INTRODUCTION

Over the years there has been a continuous commitment within the helicopter community to predict the magnitude and distribution of induced velocities in the rotor flow field with increasing precision. Most of the effort has been directed to the investigation of steady rectilinear flight but work has been done on the effects of dynamic inflow on aircraft response in the hover using modified momentum theory[1,2,3,4] and in forward flight using Glauert type non-uniform inflow[5,6]. Extensive wind tunnel work in the United States, using laser velocimetry, has resulted in inflow distribution measurements, both radially and azimuthally, for a model rotor in forward flight[7]. With the requirement to exploit and enhance the manoeuvrability of the helicopter in nap-of-the-earth flight there is the need to extend our wake modelling further into this area. The Research Instrumented Blade (RIB) on the Puma test vehicle and the continuous recording and test techniques used at RAE Bedford were developed specifically to cover transient and manoeuvring flight.

A comprehensive series of flight tests has been flown and recorded and a data reduction program is under continuous development. Some of the results obtained during hovering flight, including step input changes in collective pitch, have already been reported[8].

The main thrust of this paper was originally intended to cover local incidence distribution. In the event, much of the paper is devoted to the validation of the techniques used although incidence distribution is included and indeed affected by consideration of the techniques and accuracies obtained.

In summary, the technique depends on the use of leading edge pressure measurements and derived coefficients to obtain normal force coefficient, C_N , and incidence, α , using a comprehensive look-up table prepared from two-dimensional wind tunnel data with suitable allowance for the various unsteady effects. The method is applicable in attached flow only and the limits of applicability are delineated by the automatic detection of trailing edge pressure divergence (associated with flow separation) indicated by trailing edge sensors.

The results obtained show certain anomalies and possible inaccuracies and these are important because they throw some light on, and at best indicate areas of departure from, two-dimensional flow on which most prediction methods are based.

The general aim of the work is to support improvements to the representation of the rotor dynamics in the RAE generic simulation model.

The present paper discusses the distribution of aerodynamic loads in hover at a variety of rotor thrust coefficients and examines their consistency with aircraft load factor and measured blade root motion. Also, the data are compared with the results from a detailed rotor loads program[9]. Anomalies and their causes are also discussed. The effect on the load distribution during a transient manoeuvre from hover are examined and a brief investigation of the inflow derived from these results is made.

2 FACILITIES

The Aerospatiale Puma helicopter (Fig 1) used at RAE Bedford for flight tests is a comprehensively instrumented aircraft. An on-board PCM digital data recording system records aircraft and blade data in flight. Air data were derived from a pitot-static head, incidence and sideslip vanes, all mounted on a noseboom. These were supplemented during hover by techniques described later. Cockpit inceptor positions were measured, and a pack of inertial sensors (attitudes, rates, accelerations) provided aircraft motion data. Blade root motions (flap, lag, and feather) were measured by means of potentiometers on all four main rotor blades. One of the main rotor blades, the RIB (Fig 2), was instrumented with a total of 26 pressure sensors and 10 strain gauges. The leading edge pressure gauges were mounted at the 2% chord positions, in small smooth recesses on the metal blade upper surface, to keep disturbances of the local airflow to a minimum. The dimensions of these recesses are within the normal blade damage repair limits, so no reduction of the normal fatigue life of the blade is caused by the modification. Trailing edge sensors at the 98% chord position are locally blended into the upper surface by fairings, the flow in this region being

Fig 1 RAE Bedford Puma research helicopter

relatively unaffected by the minor change in the local shape. Wiring connections to the hub-mounted amplifiers are in a thin loom on the lower surface, blended in to the rear of the normal anti-erosion strip. small blade balance adjustments are made by changes to the blade tip balance weights, so that, overall, the instrumented blade can be considered similar both aerodynamically and dynamically, to a standard Puma blade. Details of the recording system can be found in Ref 10. Details of the derivation of blade loading and deformation are given in section 3 of this paper.

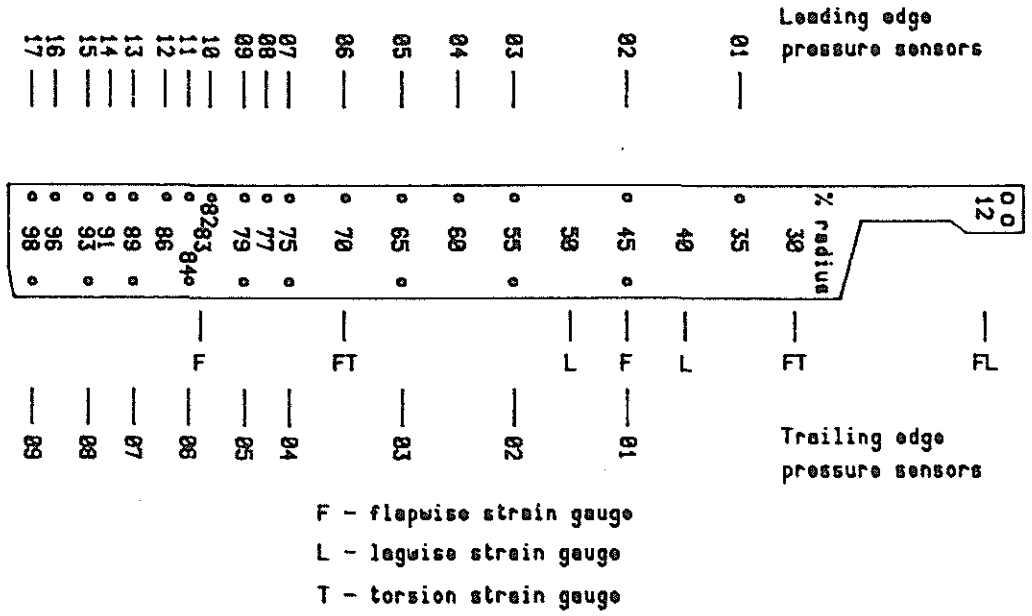

Fig 2 RIB instrumentation configuration

The most difficult aspect of the hover and hover step test flights was the capture of the hover condition itself. The aircraft had no low airspeed sensor and flights were conducted at altitude to ensure smooth conditions. A typical flight would be conducted well out of ground effect, with only the occasional cloud as a reference to low air speed transition. The method, much practised at RAE in past work, was as follows; the test pilot was guided into the hover by the flight test observer who suspended a lead ball on a 50ft long tether through the cargo hatch in the floor of the aircraft. The orientation relative to the aircraft of the line formed by the tether, served to guide the pilot into a free air hover. Any bowing of the tether indicated the direction in which the aircraft was drifting. The recording system was in continuous operation, and after the hover was obtained, a collective step input was then applied so that both a steady hover and a step input were obtained in succession. The hover tests conducted were for the range of thrust coefficients, C_T/σ , from 0.06411 to 0.09083, where σ is the rotor solidity.

3 RESUMÉ OF RIBAN

The Research Instrumented Blade ANalysis (RIBAN) package is described in detail in Ref 10, but a brief description is given below.

3.1 C_N AND INCIDENCE

The methods used to derive C_N and α and also the corrections for unsteady flow are described in Ref 10, but an outline and some additional comments are included here for completeness.

The main rotor mounted pressure sensors positioned near the leading and trailing edges are used to derive local blade normal force coefficient, C_N, and incidence, α, and to detect blade stall, respectively.

The look-up table mentioned previously was compiled from steady wind tunnel tests on the NACA 0012 aerofoil section and exists in two versions; transition fixed and transition free, either of which may be selected in the program. The differences are relatively small with the transition free data giving a higher C_{Nmax} at low Mach Number. The actual Puma blade differs slightly from the test section in terminating in a trailing edge tab (4% chord (c) in length) and having a thin anti-erosion strip slightly proud of the section proper, over the first 11% of the chord. Based on the total chord, the section is slightly thinner than the NACA 0012 overall and slightly thicker at the 2% c position. These differences should be borne in mind when reviewing the results, but are not considered to cause significant errors. Entry into the look-up table is via leading edge pressure coefficient, $C_{P_{LE}}$ and local Mach Number, M.

The derivation of C_N and α which result from this process are not applicable for conditions of separated flow, where the relationship between C_P and C_N, at a given Mach number breaks down. The trailing edge pressure sensor results are used to indicate the presence of any such stall and the level of acceptable trailing edge pressure divergence can be pre-set.

It might be thought that unsteady flow effects will be absent in the axisymmetric environment of hovering flight, but, as will be seen later, the presence of tail rotor interference effects, main rotor vortex interaction, and any present small translational velocities would result in rapid changes of flow in the tip region of the main rotor. For this reason, an outline of the unsteady corrections is also included.

Oscillatory tests with attached flow show that α leads C_N and C_N leads $C_{P_{LE}}$. Based on constants used by Beddoes[11], C_N is derived from the static values as follows:

$$C_N = C_N(\text{static}) + T_P \dot{C}_N(\text{static}) \qquad (1)$$

where $C_N(\text{static})$ is the value read from the look-up table. In hovering flight, the value of the time constant T_P would typically represent 9° of main rotor azimuth travel at 0.5 r/R, and 5° at the tip.

The basis of the method for obtaining α from C_N rests on the assumption that C_N corresponds to the static value unless α has changed in the recent past. If, for example, α has increased, then the

static value lags the actual value dependent on the magnitude of the change, and how recent its occurrence. The deficit in apparent incidence, α', from a step change in α takes the form:

$$\Delta\alpha' = \Delta\alpha(0.165e^{-t/T_1} + 0.335e^{-t/T_2})\ (1-M^2)^{0.5} \qquad (2)$$

where T_1 and T_2 are time constants dependent on the local chordwise velocity. This expression is derived from the Wagner function and represents the circulatory component of lift only; in general this is the significant one. The impulsive apparent mass terms have shorter equivalent time constants and have been neglected.

The time history of the recent past is described by a gate of n (say 10) equations based on the expression above at (n-1) past intervals which, solved numerically, enable the corrected values of α to be determined through the (typically) 235 points of each rev, and at each radial position. Although the method is an indicial one for the present, the option chosen in the program is to apply it to the first harmonic of α' only; applied to the point by point variation in α' the result is a very 'spiky' curve.

An important consideration in this paper is the inevitable departure from two-dimensional flow at the tip. As will be seen later, the local peak of increased loading at the tip from blade/vortex interaction appears very pronounced. It is known from previous measured pressure distri-butions in hover, and from theoretical considerations[12,13] that forward loading (towards the leading edge) occurs in the tip region. This means that the value of C_N derived from two-dimensional data will be an overestimate.

3.2 DEFORMATIONS

Estimates of blade deformation are obtained using the RAE-developed Strain Pattern Analysis (SPA)[14]. This is a process whereby the strain pattern of the rotating blade is related to a set of calibration mode strain patterns for the non-rotating blade, the resulting relationship being used to synthesise blade deformations from those of the calibration modes.

3.3 INDUCED VELOCITY

The RIBAN package at RAE Bedford handles all the data output from the aircraft for incidence analysis. When incorporated with SPA, both derived incidence, α, and blade pitch angle, θ, are used to obtain the local blade velocity vector angle from the simple relationship:

$$\phi = \alpha - \theta \qquad (3)$$

The inflow contribution is the residue following subtraction of components due to flap motion relative to the aircraft and aircraft motion relative to the air[10]. The complete expression for the velocity vector angle as shown below is used for all flight cases, including the hover:

$$\phi(\bar{r},\psi) = \frac{\mu_x - \lambda - \beta(\mu_x\cos\psi - \mu_y\sin\psi) + \bar{r}\bar{\omega}_y + \bar{w}_b}{\bar{r}(1 + \bar{\omega}_x\beta) + (\mu_x\sin\psi + \mu_y\cos\psi)} \quad (4)$$

Where μ_x, μ_y, μ_z are the aircraft velocity components, normalised to ΩR, in the x, y, z body directions; $\bar{\omega}_x$, $\bar{\omega}_y$ are normalised aircraft roll and pitch rates; β is the blade root flap angle (rads); $\bar{r}$ is the normalised radial position on the blade; ψ is the azimuth angle (rads); $\bar{w}_b$ is the normalised local flapping velocity; and λ is the normalised local induced velocity.

The relevant contributions for the hover step case are as shown here:

$$\phi(r,\psi) = \frac{\mu_z - \lambda + \bar{w}_b}{\bar{r}} \quad (5)$$

ie

$$\lambda(\bar{r},\psi) = \mu_z - \phi\bar{r} + \bar{w}_b \quad (6)$$

4 RESULTS

4.1 FLIGHT CONDITIONS

As noted in section 3, the flight tests used for this paper consists of hovers and collective step inputs in the hover for a range of thrust coefficients. Table 1 shows the values of C_T/σ for each event No. of Puma flight F797. The asterisks indicate those events which included a collective step input. The cases to be considered in detail are Events 3, 8, and 18, since these cover almost all the range of available thrust coefficients and include both available step inputs. An example of a collective step input, that of Event 18, is shown in Fig 3. The step shown consists of four consecutive rotor revolutions. The first is steady hover, the next two during the application of a one degree collective step input in the upward direction, and the fourth at the resulting new collective control position.

Table 1

Details of Puma Flight F797

Event No	C_T/σ
3	0.09083
4	0.08686
5	0.08246
6	0.07816
8*	0.07564
10	0.07289
14	0.06814
18*	0.06592
19	0.06411

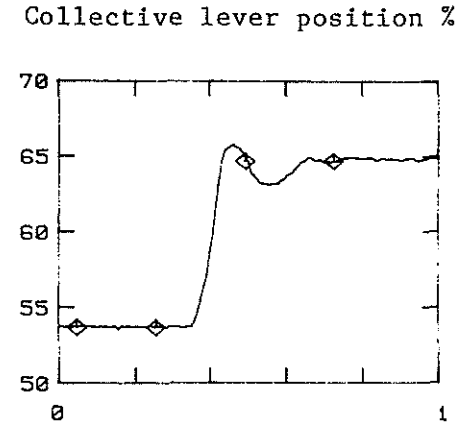

◇ - start of each rev

Fig 3 Collective lever step input

4.2 INCIDENCE AND C_N

The polar plots which follow do not present an 'instantaneous' picture, but simply a contoured, polar representation of continuous data. The view presented is from below the rotor.

Fig 4 shows the results of derived total incidence for steady hover for the three thrust coefficients, plus the four revolutions of the collective step input for Event 18. The colours and line types used for the contours joining points of equal incidence represent the same values of incidence for all six plots. Comparisons between the distributions will be made firstly for the three thrust coefficients (Events 3, 8, and 18a), and secondly for the four revs of the step input (Events 18b, c, and d).

The general trend of increasing incidence values with increasing thrust coefficient is as expected; however all three steady hover cases show several important features. Firstly, in all three cases, there is a marked uniformity of incidence distribution over at least 80% of the radius. Outboard of this there exists a loading peak, most dramatically in Event 18. For this lower thrust coefficient case, this peak caused by interaction with the trailing vortex from the previous blade occurs around 80% of the rev, and is only reduced in the region where interaction between main and tail rotor is likely to occur[15]. In the other two cases, the proportion of the rev for which this interaction is strong is considerably reduced. A closer inspection of all three Events reveals that this proportion is decreasing with increasing thrust coefficient. Ref 4 claims that the level of tip vortex interaction captured in Event 18 is a good indication of the accuracy achieved in holding the aircraft in a free air hover. This seems to be a reasonable assumption, but would cast doubt on the accuracy of hover achieved in Events 3 and 8. Indeed it appears at first sight that there may be some drift away from hover in these two Events; slightly to aft and to port. However, it may also be the case that at the higher thrust coefficients, the sharpness of the loading peak becomes diminished. The same procedure and care was taken to achieve the hover condition in all cases; if the higher thrust coefficient cases are indeed less axisymmetric than Event 18, it would indicate the sensitivity of the distribution of incidence to any small aircraft relative transition from the hover condition, particularly at the higher thrust coefficients.

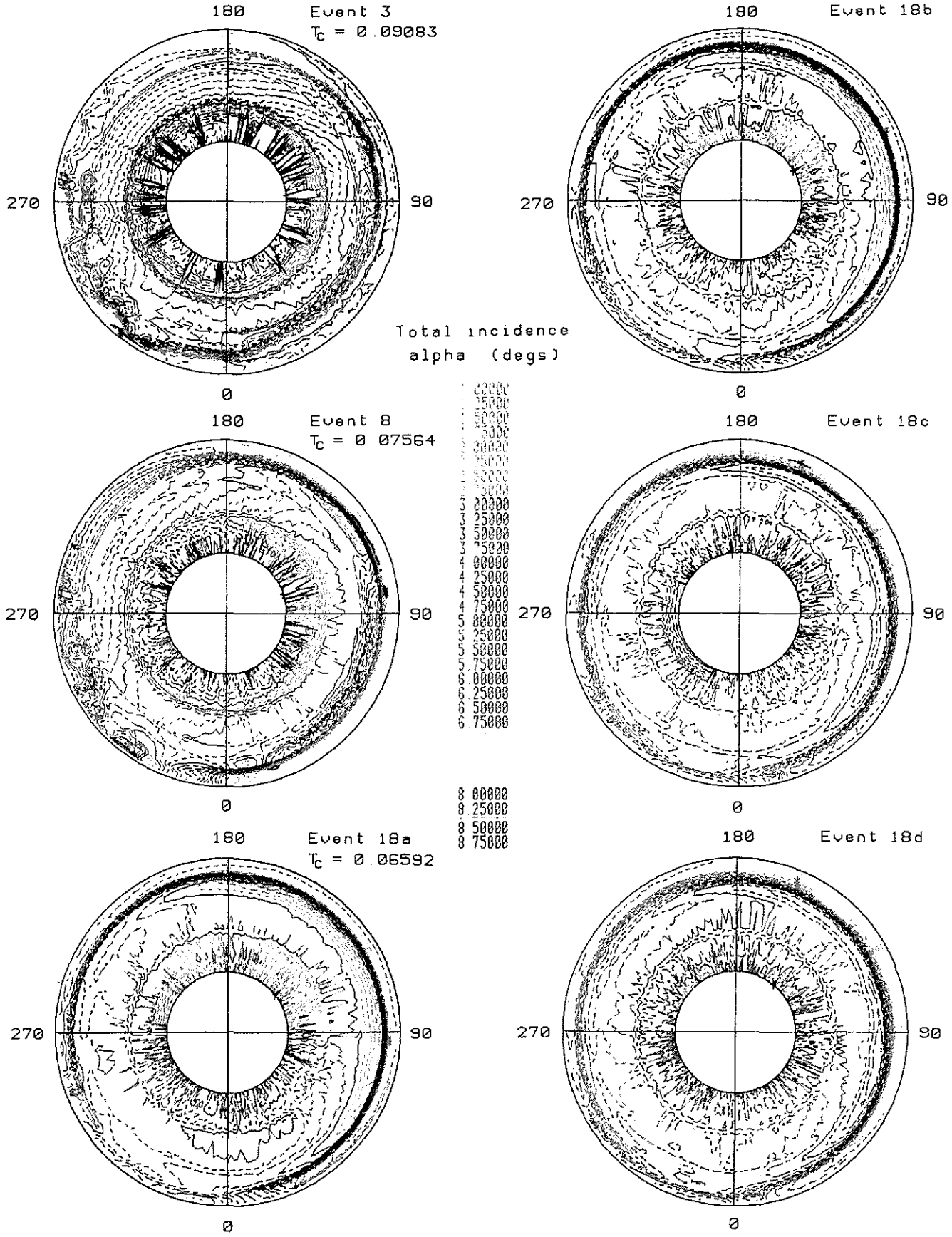

Fig 4 Contour plots of derived total incidence

With regard to the hover step, the four distributions of incidence all show similar features, and the increase in incidence, and hence loading, is apparent throughout the step.

Before proceeding with further calculation using these derived distributions of incidence, it is important to validate them as far as possible. The distribution of blade loading, C_N, is derived prior to derivation of incidence, α[10]. The distribution of C_N can be used in integration to obtain the instantaneous blade air loads. Using the (typically) 235 samples per rev these loads can be time-averaged to obtain the overall rotor thrust and moments which are the principal forces available to support and accelerate the aircraft. This process enables the load factor so derived to be compared with the appropriate aircraft normal accelerometer readings. Also, the moments about the flapping hinge so derived should be consistent with the measured blade flapping angles.

Fig 5 shows the forces on an element of rotor blade at a flap angle of β, where r is the radial position on the blade from the centre of rotation, and m is the mass per unit length. The lift on one blade at azimuth position ψ is given by:

$$L(\psi) = \tfrac{1}{2}\rho\Omega^2 \int_{eR}^{R} c(r)C_N(r)r^2\cos\beta\cos\theta dr \qquad (7)$$

where θ is the blade pitch angle (assuming rigid blade motion).

Assuming chord $c(r)$ constant, and using $\bar{r} = rR$,

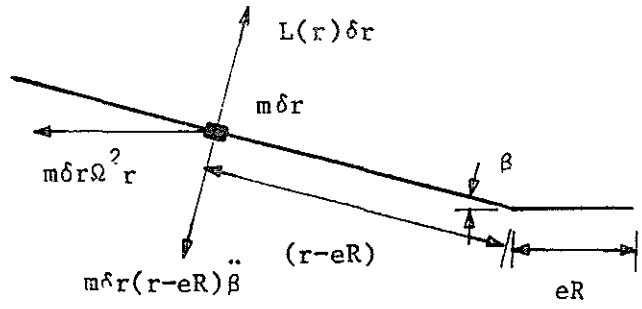

Fig 5 Forces on an element of rotor blade

$$L(\psi) = \tfrac{1}{2}\rho\Omega^2 cR^3\cos\theta\cos\beta\int_{e}^{1} \bar{r}^2 C_N(\bar{r})d\bar{r} \qquad (8)$$

For b blades,

$$L = \frac{b\rho\Omega^2 cR^3}{4\pi}\int_{o}^{2\pi}\int_{e}^{1} \bar{r}^2 C_N(\bar{r})d\bar{r}\cos\theta\cos\beta d\psi \qquad (9)$$

Taking moments about the flap hinge:

$$\int_{eR}^{R} L(r)(r-eR)\cos\theta dr = \int_{eR}^{R} m\Omega^2 r(r-eR)\beta dr + \int_{eR}^{R} m\Omega^2 (r-eR)^2 \ddot{\beta} dr \qquad (10)$$

$$= \Omega^2 \beta_o (I_\beta + M_\beta eR) + M_\beta \Omega^2 eR(\beta_{1c}\cos\psi + \beta_{1s}\sin\psi) \qquad (11)$$

where $\beta = \beta_o + \beta_{1c}\cos\psi + \beta_{1s}\sin\psi$

$$M_\beta = \int_{eR}^{R} m(r-eR)dr$$

$$I_\beta = \int_{eR}^{R} m(r-eR)^2 dr$$

The values of both first and second moments of mass were calculated from a mass breakdown of a standard Puma blade.

Hence, for a clockwise rotor:

$$M_o = 1/2\pi \int_o^{2\pi} \int_e^1 L(\bar{r})\ (\bar{r}-e)R^2\cos\theta d\bar{r}d\psi = \Omega^2\beta_o(I_\beta + M_\beta eR) \qquad (12)$$

$$M_{1s} = 1/2\pi \int_o^{2\pi} \int_e^1 L(\bar{r})\ (\bar{r}-e)R^2\cos\theta\sin\psi d\bar{r}d\psi = M_\beta\Omega^2 eR\beta_{1s}/2 \qquad (13)$$

$$M_{1c} = -1/2\pi \int_o^{2\pi} \int_e^1 L(\bar{r})\ (\bar{r}-e)R^2\cos\theta\cos\psi d\bar{r}d\psi = M_\beta\Omega^2 eR\beta_{1c}/2 \qquad (14)$$

The expressions for the thrust and coning moment are valid for both steady conditions and manoeuvring flight; however, those for M_{1s} and M_{1c} are invalid for manoeuvring flight including pitch and roll motion since the blade gyroscopic moments are not included.

In addition, the C_N distribution can be integrated to examine the overall change in the thrust and moment results, when the transition free as opposed to transition fixed wind tunnel results are used, with the application of a lead between C_N and leading edge C_P, and with the application of empirical correction factors, to tip loading results for example. The results for the moments can be used to derive the coning and first harmonic flap angles (assuming rigid blade motion) for comparison with those derived from the measured root flap angle.

Despite a limited number of sensor positions being used, for

Table 2

Baseline results for flight F797

	Event 3		Event 8		Event 18	
	Measured	Derived	Measured	Derived	Measured	Derived
Thrust/ Weight(N)	55770	58553	54593	57827	53415	57517
β_o (degs)	3.497	5.068	3.410	4.936	3.330	4.842
β_{1c} (degs)	-3.087	-6.115	-3.407	-6.191	-2.596	-4.005
β_{1s} (degs)	0.810	1.061	0.558	-0.574	0.141	-0.937

radial positions between 0.35 and 0.98 r/R, all the integrations were performed from the root cut-out at 0.25 r/R to the tip. It was assumed that the value of C_N was zero at both these points, and that the value of C_N between these points and their neighbouring sensor positions varied linearly with radius.

Results for the baseline run (static C_N, transition fixed, no correction factors) are contained in Table 2. The table shows the results for total thrust in the tip path plane, and flapping angles derived from the moments about the flapping hinge, in the shaft axis. Also shown are the aircraft weight, and the flapping angles calculated from the measured root flap angle.

Before comparing measured and derived results in detail it is worth confirming that the derived results follow the trend of those measured. Indeed it is quite clear that the overall thrust and coning angle all increase with thrust coefficient as would be expected; however it is worth noting that the value of β_{1c} does not follow a recognisable trend, although the derived result follows the trend of that measured, in that its value first becomes more negative from Event 18 to Event 8, but then increases positively from Event 8 to Event 3. The trend of increasing β_{1s} with thrust coefficient is followed by both sets of data.

The thrust results all overestimate the aircraft weight by some 5% which is an acceptable value to account for fuselage download. It must be pointed out that the accuracy of the 'measured' results can only be expected to lie within ±5%, however. The values for coning angle overestimate the measured values significantly, errors being about 20%. Part of the error in coning can be attributed to the fact that it is not the rigid blade flapping which is measured at the root, but a combination of mostly rigid, plus some elastic flapping motion. The calculation to derive the coning angle assumes rigid blade motion; the elastic content in the root motion indicates that the real rigid flapping displacements are

in excess of the total flapping displacement, although this only removes some 10-12% of the error of the derived value of β_o . This indicates that the tip loading may be overestimated as described in section 4.1. The results for the first harmonics of flapping cannot be relied upon; the derivation of pitching and rolling moments by integration are critically dependent on the magnitude and distribution of radial loading. For example, one degree of first harmonic flapping represents less than 1% of mean aerodynamic moment.

Table 3 summarises the results of the integration process for five calculation conditions, for the three steady hovers. These conditions are as follows:

A Transition fixed, Static C_N

B Transition free, Static C_N

C Transition fixed, C_N with lead

D Transition fixed, Static C_N, Constant tip C_N factor

E Transition fixed, Static C_N, Variable tip C_N factor

Table 3

Errors in results for flight F797 (%)

Event		Thrust	β_o	β_{1c}	β_{1s}	β'_o	C_T/σ
3	A	5.1	44.9	98.1	31.0	33.1	0.09083
3	B	-3.0	33.1	88.0	-202.4	22.2	
3	C	5.1	44.9	77.9	67.6	33.1	
3	D	-17.6	8.9	80.0	-277.4	0.0	
3	E	-16.7	9.4	90.9	-274.4	0.4	
8	A	6.0	44.8	81.7	-204.8	33.6	0.07564
8	B	-0.1	35.9	46.2	-406.7	25.4	
8	C	6.0	44.8	55.5	-204.2	33.6	
8	D	-16.9	8.3	16.6	-716.2	-0.1	
8	E	-16.7	7.8	10.6	-864.5	-0.5	
18	A	7.7	45.4	54.2	-764.8	34.7	0.06592
18	B	3.4	39.2	-11.3	-1356.6	28.9	
18	C	7.7	45.4	48.9	-632.2	34.2	
18	D	-14.9	9.1	-117.0	-1619.9	1.1	
18	E	-15.5	7.6	-57.0	-2202.6	-0.3	

The two types of tip factor (conditions D and E) are empirical correction factors to examine the change in thrust when derived coning angle is artificially factored to give a favourable comparison with the measured value. This is an attempt to discover where any errors in

derived C_N may lie, as will be seen. The first factor is a constant one, set to 0.54, applicable outboard of a pre-set radial position (0.89 r/R). The second is a factor proportional to radius with respect to a pre-set position (0.89 r/R); the factor is set to 1.0 here, and varies linearly to 0.0 at the tip.

The results in Table 3 are presented as the percentage error between the values derived from the C_N data, and the measured data. β'_o represents the rigid blade value of the coning angle (total flap angle - elastic flap angle).

The major features indicated by the results in Table 3 are the trend in the errors of the parameters with variation of thrust coefficient, inclusion of C_N lead and transition free data, and the corrections needed to attain an acceptable degree of accuracy for the derived coning angle.

As thrust coefficient is increased, it can be seen that the error in the calculated thrust decreases steadily, whereas the result for β_o changes little, although that for the true, rigid blade coning angle decreases also. The results for the first harmonics of flap show opposite trends between β_{1c} and β_{1s}, but the errors are certainly obtrusive.

The application of the transition free results reduces the calculated values of thrust and coning angle, the effect on the error increasing with thrust coefficient, to the point that the thrust result is less than the weight, for Events 3 and 8.

The inclusion of the lead of C_N over leading edge pressure does not affect the results of thrust, or coning, to any significant degree. In this case, the lead has only been applied to the first harmonic of C_N, to reflect changes in C_N due to changes in pitch alone, and this component is relatively small in hover, but becomes significant in forward flight.

The changes in errors due to application of tip factors need some explanation. In both types of correction, the value of the factor, and/or position at which the factor(s) are applied, were set by trial and error in order to artificially set the derived value of coning angle to that of the rigid blade value. It can be seen that in both cases, the correction position was 0.89 r/R, and both this position and the factor of 0.54 for the first case were kept constant for all three thrust coefficients. In both cases, the resulting thrust was reduced to an unacceptable degree, well below the value of the weight, for all three Events. The two methods did not give radically different results when compared to each other, so the simple constant factor method would suffice for future use. It is sufficient to point out that in order to obtain acceptable degrees of accuracy for both the thrust and coning angle, the distribution of C_N must be reconsidered; it appears that there is some error in the inboard distribution, since correction of the tip region where errors are expected does not account for the differences.

Fig 6 shows a comparison of the flight results of C_N for Event 18a with those of the RAE/WHL loads program. The loads program for hover gives an axisymmetric distribution of C_N over the rotor disc; the flight derived results shown are averaged to give a suitable comparison. It can be seen that the program results indeed give a reduced estimate of C_N in the tip region, but the thrust is maintained by the increased level inboard.

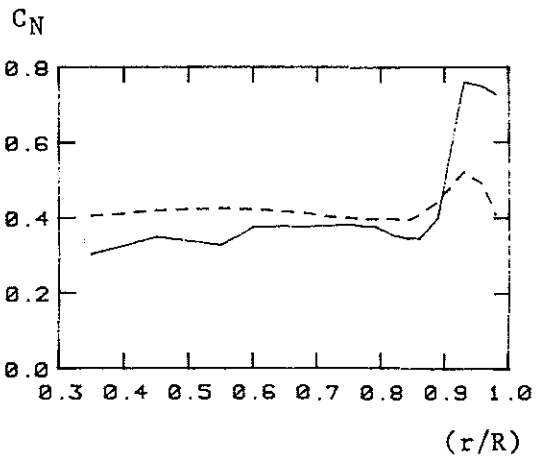

——— - average flight results
---- - loads program results

Fig 6 Comparison of averaged flight results with those of the RAE/WHL loads program

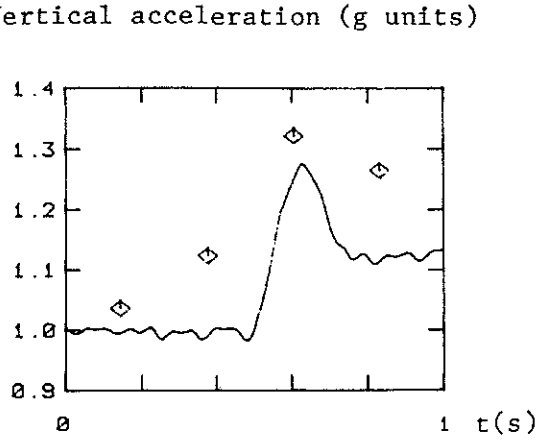

◇ - integrated values
——— - aircraft response

Fig 7 Validation of incidence and load analysis - comparison of disc mean integrated loads with normal acceleration.

The same process of integrating the C_N data for the steady hover cases was also used for the hover step of Event 18. In this case, the ratio of the calculated thrust to the aircraft weight is compared to the normal acceleration in 'g' units; the results for the four revs of this step are shown in Fig 7. The results are those for transition free, C_N with lead, and no tip correction factors.

The discrepancies that are apparent may be due to several possible effects. Firstly, the integrated loads are averages over each rev, during which, as the normal acceleration response shows, the load factor may change significantly eg, 1.0g to 1.27g during the third revolution (Event 18c). Secondly, during collective control activity, the resulting blade flap motion, and change in rotor thrust tends to lead the aircraft vertical acceleration response. The inclusion of the C_N with lead again made no noticeable difference to the results, and the use of the transition free data tended to reduce the factors obtained from using that for transition fixed, consistent with the results for the steady hover cases.

4.3 INDUCED VELOCITY

As mentioned in section 3.3, the derived values of induced velocity, λ , depend on those derived for the incidence, α . Despite the inconsistencies found to be present in the C_N data, which is also derived from the incidence data, it is felt worthwhile to provide the results obtained thus far from the derivation of induced velocity for one of the flight cases. Fig 8 shows the results for the steady hover case in Event 18, in an isometric format (downwash positive, upwash negative). As for the incidence, the majority of the distribution is featureless in comparison to the effects of the tip vortex. For the majority of the distribution, ie to 0.86 r/R, the induced velocity takes the form of downwash in the uniform, momentum theory predicted manner, with the airflow being convected downwards as it approaches the blade. However, in the tip region, the influence of the tip vortex gives rise to a pronounced decrease in inflow as the tip is approached, to the point that an upwash replaces the downwash. This is consistent with the increased tip loading as shown

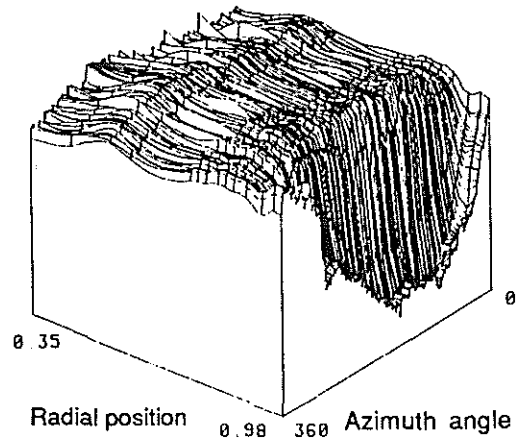

max = 0.0725
min = -0.0297

Fig 8 Surface plot of derived downwash during steady hover

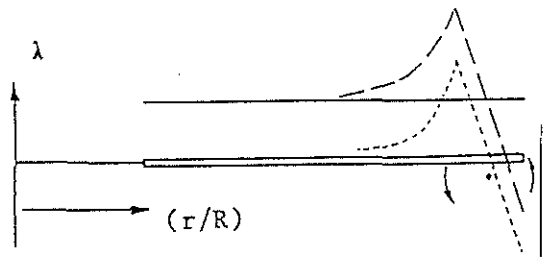

——— momentum theory distribution (ideal rotor)
----- tip vortex distribution
– – – momentum theory with tip vortex

Fig 9 Schematic showing influence of tip vortex on downwash

previously. Fig 9 shows a simplified view of how such a tip vortex downwash distribution can be superimposed on that predicted by simple momentum theory. Although the abrupt decrease in downwash outboard of the vortex core is well represented in the derived data, the increase in downwash inboard of the core is not nearly so obvious. On the first point, the loading peak at the tip may be exaggerated as discussed in the previous section; a reduction of this loading and its related incidence would increase the downwash at the tip. On the second point, one explanation is provided by examination of the tip vortex history. As the tip vortex from the preceding blade is convected inwards and downwards, its effect on the lift distribution near the tip is to reduce the downloading effect of the 'new' tip vortex, thus reducing the peak in downwash inboard of this vortex core.

Fig 10 shows an isometric display of downwash for the whole of the step input of Event 18. It can be readily seen that the shape and form of the downwash distribution is retained throughout the transient response to the manoeuvre, including the apparent tail rotor interference effects towards the end of each rev.

4.4 BLADE MOTION

Before discussing the results further, it is important to identify the contributions to the derived induced velocity, of both rigid and elastic blade motion. Equation (6) shows that in hover, only the inflow angle and flap velocity (due to cyclic pitch referred to the tip path plane) are significant when viewed in the shaft axis. Moreover, numerically, these contributions have an equal significance over a substantial proportion (up to 50%) of the disc.

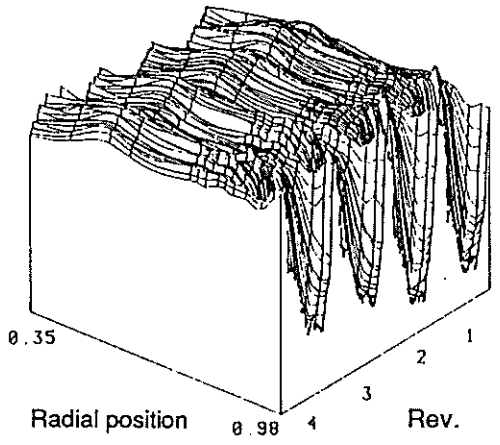

max = 0.0795
min = -0.0297

Fig 10 Surface plot of derived downwash for subsequent rotor revolutions during step input

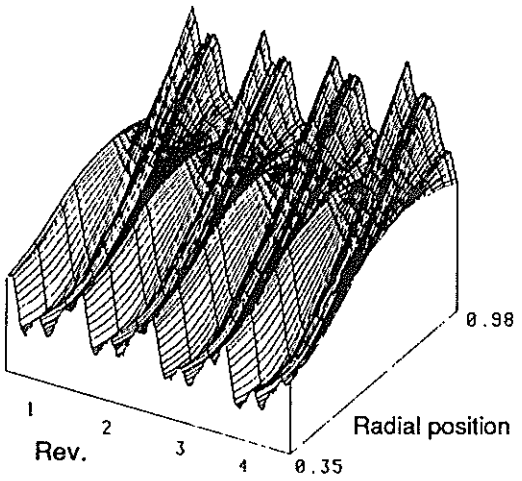

max = 34.6
min = -32.0

Fig 11 Surface plot of derived blade elastic flap displacement during step input

The accuracy to which the local blade pitch angle is derived can affect the resulting derived inflow significantly. The local pitch angle is composed of both rigid and elastic components. Now, there are only two strain gauges on the RIB used to derive the elastic pitch displacement; recent work suggests that this could be insufficient for confidently and accurately deriving elastic pitch[16]. Pitch angle measurements are limited here to those measured at the blade root. However, results of work undertaken at RAE Farnborough with an extensively strain gauged Puma rotor blade in hover show that elastic pitch angles of +1.5° at the tip may be typical[14]. When a linear distribution of pitch, with a value of -1.5° at the tip, was included in the derivation to represent elastic pitch, changes of up to 15% in the resulting inflow distribution were apparent. It is thus concluded that inclusion of elastic pitch measurements in the analysis is important. As a result of this, another SPA calibration is being carried out; any resultant changes to the derived data will be reported later[16].

The flap displacements used to calculate the flap velocities are also made up of both rigid and elastic components, the second of which accounts for up to 5% of the total flap displacement[16]. Fig 11 shows the elastic flap displacements as an isometric plot, for the whole collective step. Minimum and maximum values in millimetres are shown as a guide to scale.

5 DISCUSSION AND CONCLUSIONS

This paper has sought to derive the distribution of incidence and blade deformation on a Puma helicopter in hover with the intention of examining the differences between the theoretical distribution of induced

velocity and that existing in practice. In the event, considerable attention has been given to the validation of results particularly with regard to the integrated aerodynamic forces and moments and their consistency with separately measured aircraft load factor and blade motion.

The method used to derive aerodynamic blade loads depends on an interpretation of leading edge pressure coefficient in assumed two-dimensional flow. Inconsistencies and anomalies are instructive in indicating where this breaks down. Although not reported, these effects are now being examined in the wider context of forward flight, including manoeuvres.

The trends of incidence distribution with thrust coefficient both statically and during the transient application of collective pitch, are largely as expected in that the distribution remains essentially constant, apart from the region of tip vortex interaction, but the magnitude increases with thrust coefficient. The departure from an axisymmetric distribution occurs in the region of the efflux from the tail rotor, but the overall distributions are sensitive to small translational velocities of the helicopter. The following conclusions are drawn:

1 Apart from the region near the efflux from the tail rotor, the distribution of incidence was essentially uniform except in the tip region where the effect of blade/tip vortex interaction, causing increased loading, was very pronounced. the forward loading known to occur in the tip region leads to some overestimation of the lift in this area with the technique used. As the overall integrated rotor thrust is, as expected, slightly greater than the weight, it can be inferred that inboard lift is underestimated. If so, the reason for this underestimation is not understood.

2 Unsteady effects are incorporated into the data reduction program but their effect during hover on overall thrust and moments was small and consistent with the relatively small asymmetries in loading relative to those occurring in forward flight.

3 The derivation of blade incidence together with the blade deformations and the aircraft motion allows an estimate of the resulting local induced velocity to be made. Following from (1), in steady hover, the downwash was uniform inboard but in the tip region the value of the downwash decreases drastically due to the effects of blade/tip vortex interaction. Even during hover the contribution of elastic deformations to derived induced velocity was appreciable.

4 Further analysis over a range of speeds in forward flight and during manoeuvring flight is required before the full potential of the methods used can be assessed, and this is proceeding.

REFERENCES

1) P.J. Carpenter, Effect of a rapid blade-pitch increase on the thrust and induced-velocity response of a full-scale helicopter rotor. NACA Technical Note 3044, 1953.

2) D.M. Pitt, D.A. Peters, Theoretical prediction of dynamic-inflow derivatives, Vertica V5, No 1, 1981.

3) R.T.N. Chen, W.S. Hindson, Influence of dynamic inflow on the helicopter vertical response, Vertica V11, Nos 1 and 2, 1987.

REFERENCES (concluded)

4) S.S. Houston, P.C. Tarttelin, Theoretical and experimental correlation of helicopter aeromechanics in hover, Paper presented at 45th American Helicopter Society National Forum, Boston, May 1989. (RAE TM FM 20)

5) R.A. Ormiston, D.A. Peters, Hingeless helicopter rotor response with non-uniform inflow and elastic blade bending, Journal of Aircraft V9 No 10, 1972.

6) G.D. Padfield, A theoretical model of helicopter flight mechanics for application to piloted simulation, RAE Technical Report 81048, 1981.

7) J.W. Elliot, S.L. Althoff, Inflow measurement made with a laser velocimeter on a helicopter model in forward flight, NASA Technical Memorandum 100541-5, 1988.

8) P.C. Tarttelin, Report on HTP-6 Workshop on parameter identification, RAE unpublished paper.

9) C. Young, Development of the vortex ring wake model and its influence on the prediction of rotor loads, AGARD CP334, 1982.

10) M.J. Riley, et al., Estimation of rotor blade incidence and blade deformation from the measurement of pressures and strains in flight, Paper presented at 14th European Rotorcraft Forum, Milan, Sept. 1988.

11) T.S. Beddoes, Representation of airfoil behaviour, Vertica V7, No 2, 1983.

12) M.J. Riley, P.B. Brotherhood, Comparative measurements of two helicopter blade profiles in hovering flight, ARC R&M, 1977.

13) D. Küchmann, A simple method for calculating the span and chordwise loadings on straight and swept wings of any given aspect ratio at subsonic speeds, ARC R&M 2935, 1956.

14) A.R. Walker, Experimental determination of rotating helicopter blade deformations using strain pattern analysis. RAE Technical Memorandum MAT STR 1108, 1988.

15) A. Brocklehurst, Main rotor/tail rotor interactions near hover, Westland Helicopters Research Memorandum RM 535, 1986.

16) P.C. Tarttelin, Analysis of test data from the RAE Research Instrumented Blade - Part one: Hover, RAE Technical Report (in preparation).